Electronic Supplementary Information for:

Red-to-NIR Luminescent Trinuclear Gold(I) Complexes with Liquid-Crystalline Phases over an Exceptionally Wide Temperature Range

Tamon Nakao,[a†] Abhilash Sahu, [a†] Kenta Yamaguchi,[a] Arushi Rawat,[a] Kosuke Kaneko,[a‡] Kohsuke Matsumoto,[a] Ganesan Prabusankar,[b] and Osamu Tsutsumi*[a,b]

[a.] *Department of Applied Chemistry, Ritsumeikan University 1–1–1 Nojihigashi, Kusatsu 525-8577, Japan.*
[b.] *Indian Institute of Technology Hyderabad, Kandi, Telangana 502285, India.*
† *These authors contributed equally to this work.*
‡ *Present Adress: College of Liberal Arts and Sciences, Kitasato University, 1-15-1 Kitasato, Sagamihara, Kanagawa, 228-8555 Japan*

*Correspondence should be addressed to O. Tsutsumi. (email: tsutsumi@sk.ritsumei.ac.jp)

Table of content

1. Materials

The gold(I) complexes were synthesized via a facile four-step procedure starting from commercially available ethyl diacetoacetate, as outlined in Scheme 1. All solvents and reagents were of analytical grade and were used as received without further purification unless otherwise stated. ^{1}H and ^{13}C NMR spectra were recorded on a JEOL ECS-400 spectrometer (^{1}H: 395.884 MHz, and ^{13}C: 99.545 MHz) in $CDCl_3$ as the solvent. Chemical shifts are reported in parts per million (ppm) relative to the residual proton signal of the deuterated solvent. Infrared (IR) spectra were obtained using the KBr pellet method on a JASCO FT/IR-610 spectrometer and are reported in wavenumbers (cm^{-1}). Electrospray ionization mass spectrometry (ESI-MS) measurements were carried out on a Bruker micrOTOF II mass spectrometer. Elemental analyses were performed using a MICRO CORDER JM10 analyser (J-SCIENCE).

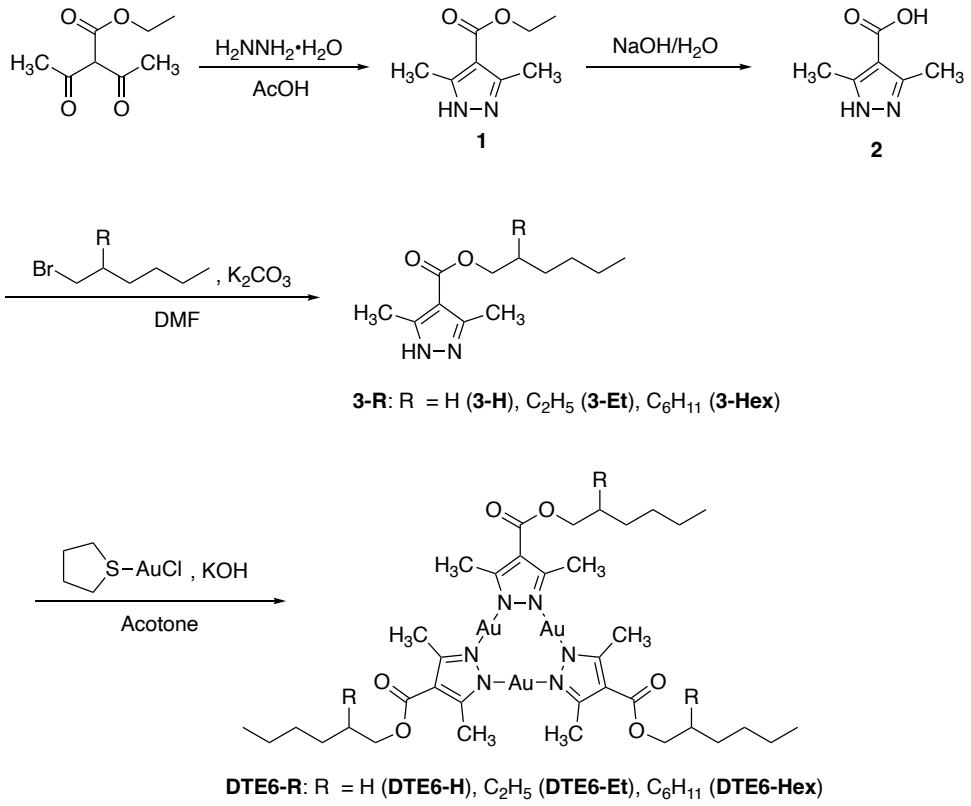

Scheme S1. Synthetic route to cyclic trinuclear Au(I) complexes bearing ester-linked alkyl side chains (DTE6-R).

Synthesis of ethyl 3,5-dimethyl-1*H*-pyrazole-4-carboxylate (1)

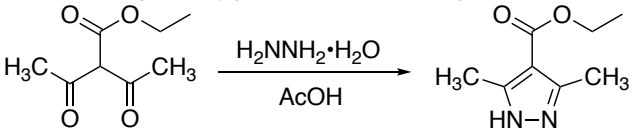

1

Ethyl diacetoacetate (0.86 g, 5.0 mmol) and hydrazine monohydrate (0.25 g, 5.0 mmol) were added to acetic acid (10 mL), and the reaction mixture was stirred at room temperature for 21 h. After completion of the reaction, the mixture was diluted with water (10 mL) and carefully neutralized with a saturated aqueous $NaHCO_3$ solution. The resulting white precipitate was collected by filtration to afford the title compound as a white solid (0.60 g, 3.6 mmol) in 72% yield. ^{1}H NMR (400 MHz, $CDCl_3$, δ): 4.30 (q, J = 7.3 Hz, 2H, $COOCH_2CH_3$), 4.25–4.01 (br, 1H, N*H*), 2.51 (s, 6H, pyrazole-CH_3), 1.36 (t, J = 7.3 Hz, 3H, $COOCH_2CH_3$).

Synthesis of 3,5-Dimethyl-1*H*-pyrazole-4-carboxylic acid (2)

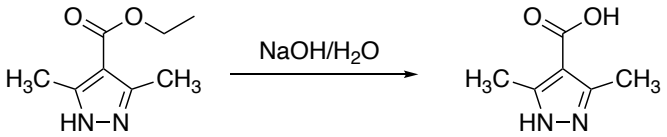

1 **2**

Compound 1 (0.50 g, 2.9 mmol) was added to an aqueous NaOH solution (0.2 mol L^{-1}), and the resulting mixture was refluxed for 12 h. After completion of the reaction, the mixture was cooled to room temperature and carefully neutralized with hydrochloric acid (1 mol L^{-1}). The resulting white precipitate was collected by filtration to afford the title compound as a white solid (0.25 g, 1.8 mmol) in 62% yield. ^{1}H NMR (400 MHz, Acetone-d_6, δ): 3.10–2.56 (br, 1H, N*H*), 2.40 (s, 6H, pyrazole-CH_3).

Synthesis of Alkyl 3,5-dimethyl-1*H*-pyrazole-4-carboxylate (3-R)

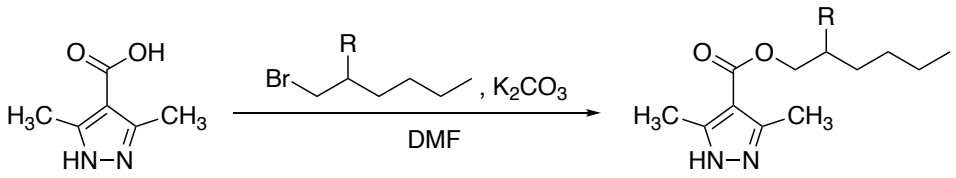

2

3-R: R = H (**3-H**), C_2H_5 (**3-Et**), C_6H_{11} (**3-Hex**)

Compound 2 (70 mg, 0.50 mmol), 1-bromohexane (0.83 g, 0.50 mmol), and potassium carbonate (0.69 g, 5.0 mmol) were added to *N,N*-dimethylformamide (DMF, 20 mL), and the resulting mixture was stirred at room temperature for 23 h. After completion of the reaction, the mixture was diluted with diethyl ether and washed successively with water and brine. The organic layer was dried over anhydrous sodium sulphate, filtered, and concentrated under reduced pressure to afford the title compound as a colourless liquid (83 mg, 0.37 mmol) in 74% yield. ^{1}H NMR (400 MHz, $CDCl_3$, δ): 5.48–5.12 (br, 1H, N*H*), 4.22 (t, J = 7.0 Hz, 2H, $COOCH_2C_5H_{11}$), 2.49 (s, 6H, pyrazoleCH_3), 1.74–1.68 (m, 2H, $COOCH_2CH_2C_4H_9$), 1.53 (quin, J = 7.3 Hz, 2H, $COOC_2H_4CH_2C_3H_7$), 1.32–1.27 (m, 4H, $COOC_3H_6C_2H_4CH_3$), 0.88 (t, J = 7.0 Hz, 3H, $COOC_5H_{10}CH_3$).

2-Ethylhexyl 3,5-dimethyl-1H-pyrazole-4-carboxylate (3-Et) and 2-butyloctyl 3,5-dimethyl-1H-pyrazole-4-carboxylate (3-Hex).

These compounds were synthesized following the same procedure as described above for 3-H. The desired products 3-Et and 3-Hex were obtained as colourless liquids in 51% and 63% yields, respectively.

3-Et: ^{1}H NMR (400 MHz, $CDCl_3$, δ): 4.30–3.90 (br, 1H, N$\underline{H}$), 4.18 (octet, J = 3.2 Hz, 2H, COOC$\underline{H_2}$CH(C_2H_5)C_4H_9), 2.50 (s, 6H, pyr-C$\underline{H_3}$), 1.66 (septet, J = 6.3 Hz, 1H, $COOCH_2C\underline{H}(C_2H_5)C_4H_9$), 1.47–1.28 (m, 8H, $COOCH_2CH(C\underline{H_2}CH_3)C_3\underline{H_6}CH_3$), 0.95-0.87 (m, 6H, $COOCH_2CH(CH_2C\underline{H_3})C_3H_6C\underline{H_3}$).

3-Hex: ^{1}H NMR (400 MHz, $CDCl_3$, δ): 4.16 (d, J = 5.4 Hz, 2H, COOC$\underline{H_2}$CH(C_6H_{13})C_4H_9), 2.49 (s, 6H, pyr-C$\underline{H_3}$), 1.71 (d, J = 11.8 Hz, 1H, $COOCH_2C\underline{H}(C_6H_{13})C_4H_9$), 1.37–1.27 (m, 16H, $COOCH_2CH(C_5\underline{H_{10}}CH_3)C_3\underline{H_6}CH_3$), 0.88 (m, 6H, $COOCH_2CH(C_5H_{10}C\underline{H_3})C_3H_6C\underline{H_3}$).

2. NMR spectra

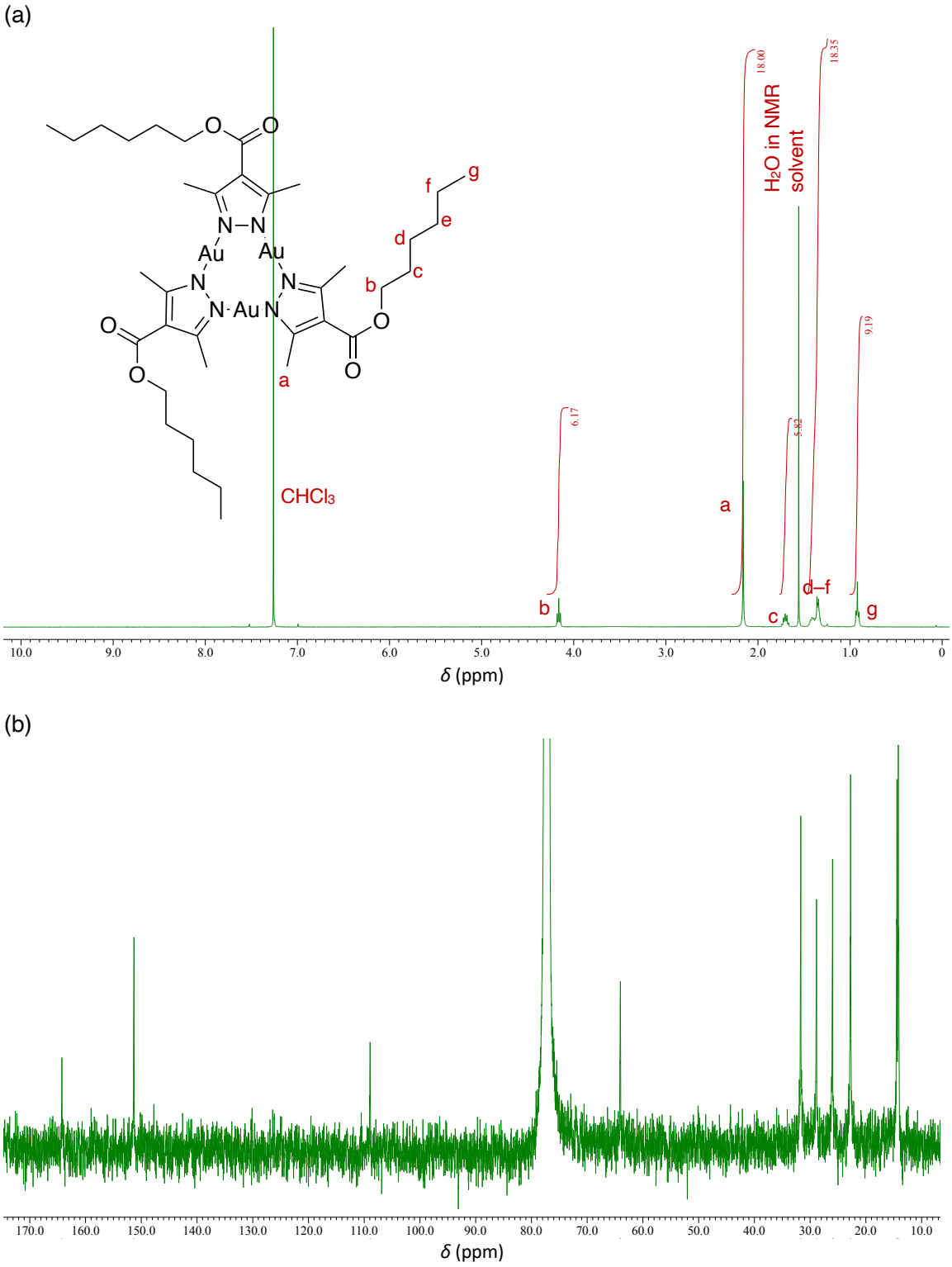

Figure S2. NMR spectra of **DTE6-H** in $CDCl_3$: (a) ^1H NMR, (b) ^{13}C NMR.

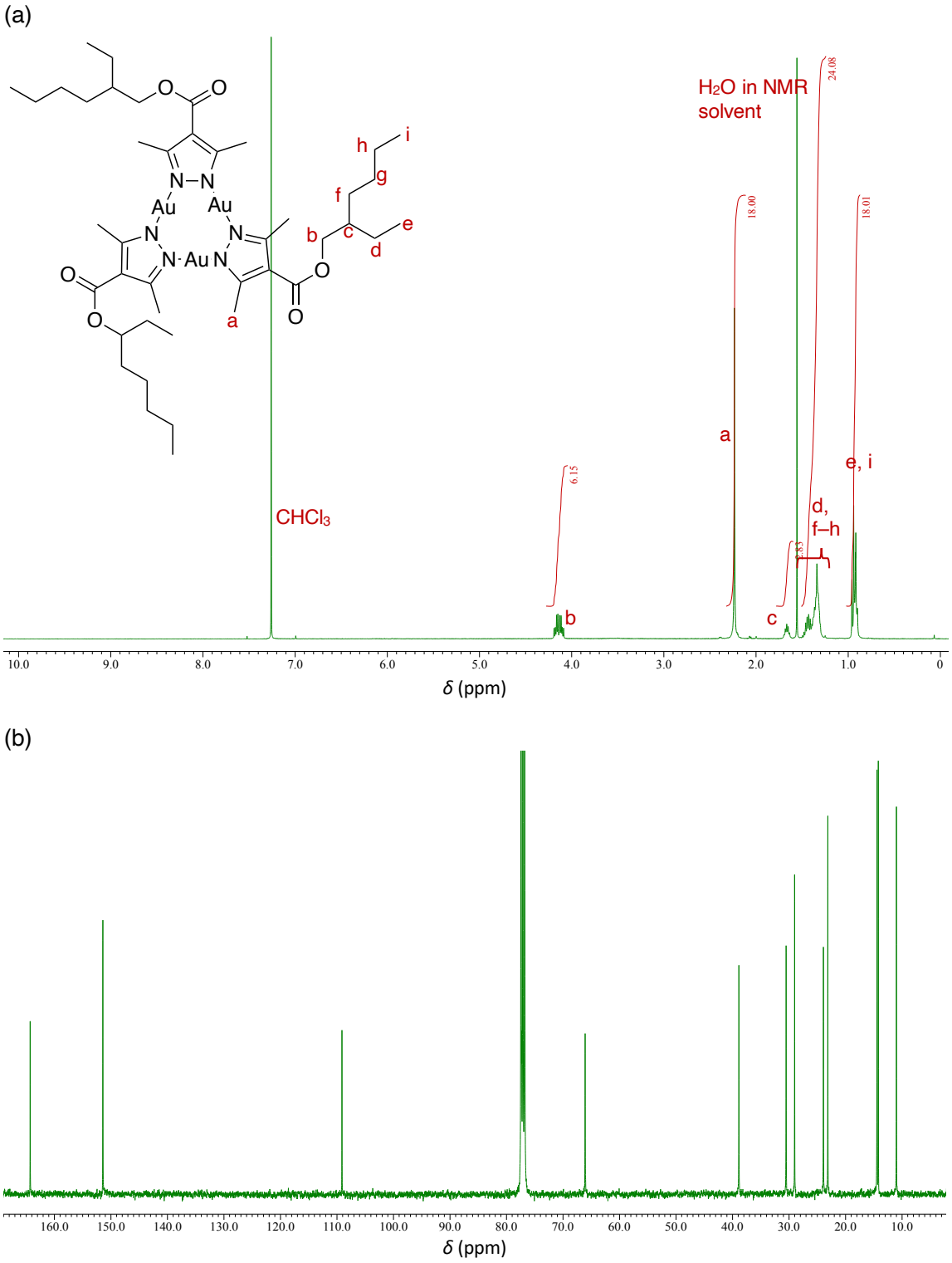

Figure S3. NMR spectra of **DTE6-Et** in $CDCl_3$: (a) ^{1}H NMR, (b) ^{13}C NMR.

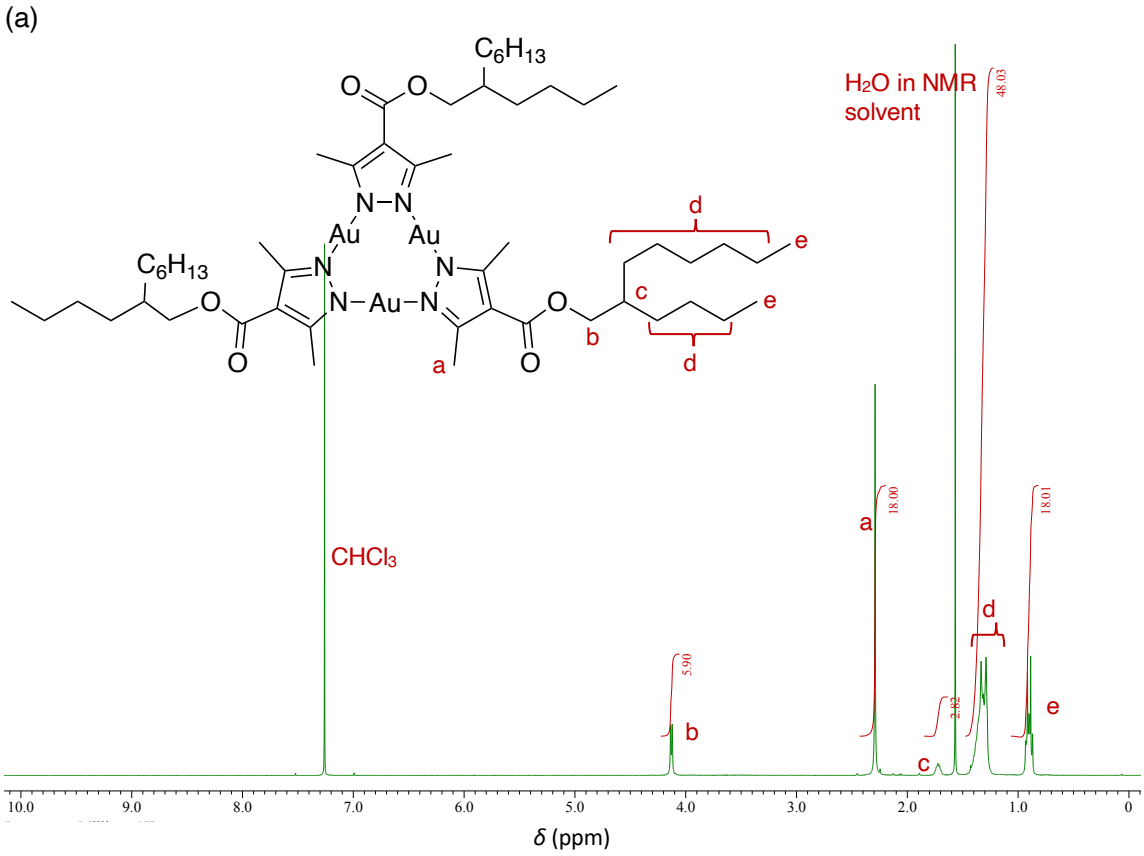

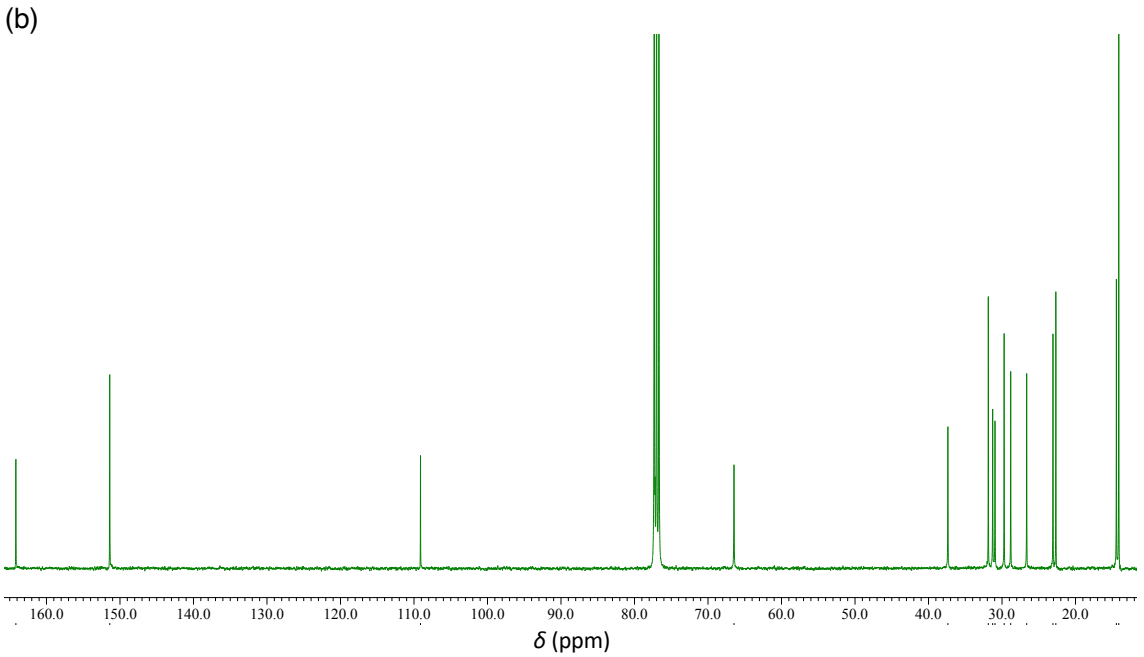

Figure S4. NMR spectra of **DTE6-Hex** in $CDCl_3$: (a) ^{1}H NMR, (b) ^{13}C NMR

3. Mass spectra

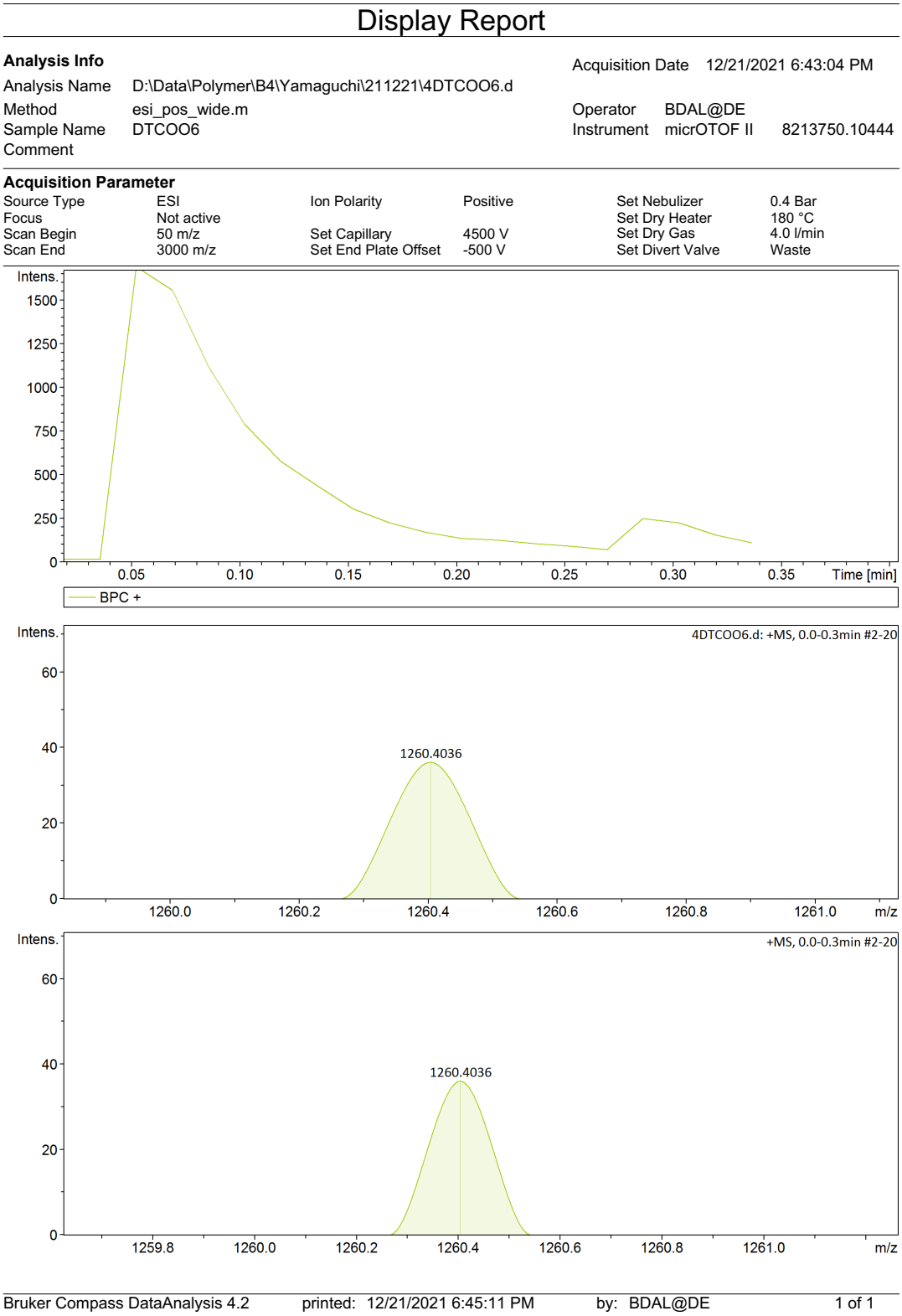

Figure S5 ESI-MS spectra for DTE6-H.

Display Report

Analysis Info

Analysis Name	D:\Data\Polymer\B4\Yamaguchi\211221\18DTCOO2EH.d	Acquisition Date	2/11/2022 6:32:34 PM
Method	DEFAULT.m	Operator	BDAL@DE
Sample Name		Instrument	micrOTOF II 8213750.10444
Comment			

Acquisition Parameter

Source Type	ESI	Ion Polarity	Positive	Set Nebulizer	0.3 Bar
Focus	Not active			Set Dry Heater	200 °C
Scan Begin	500 m/z	Set Capillary	4500 V	Set Dry Gas	4.0 l/min
Scan End	3000 m/z	Set End Plate Offset	-500 V	Set Divert Valve	Waste

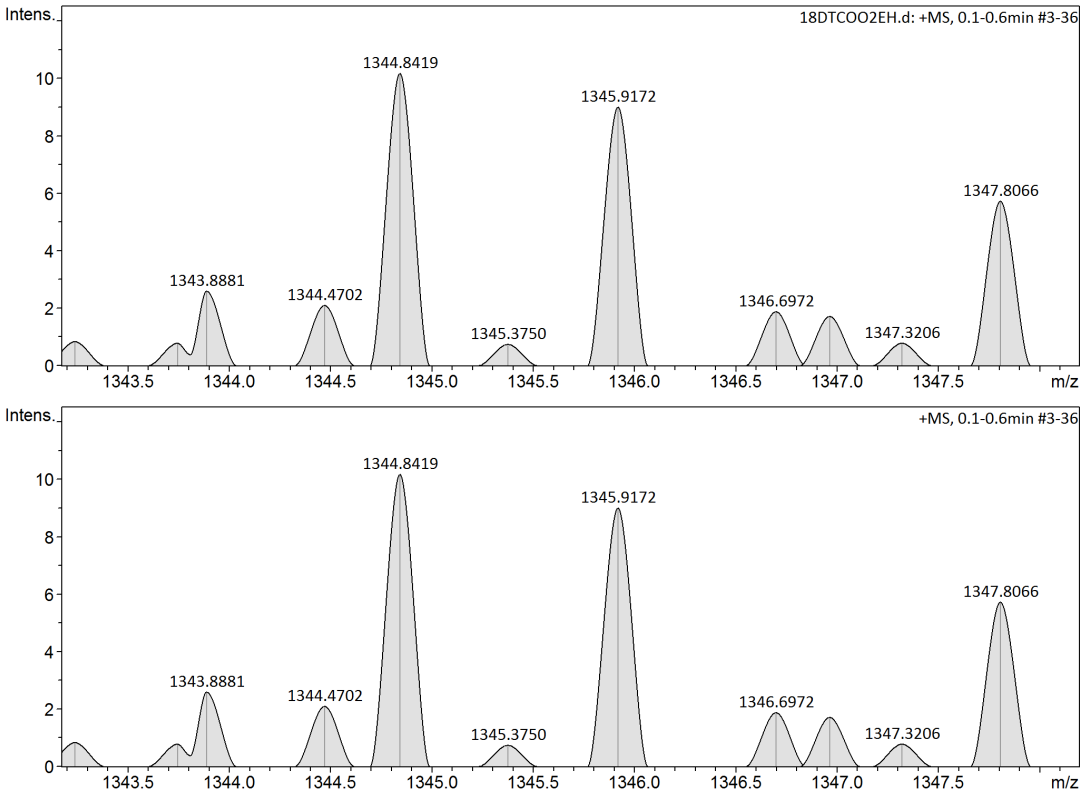

Bruker Compass DataAnalysis 4.2 printed: 2/11/2022 6:40:25 PM by: BDAL@DE 1 of 1

Figure S6 ESI-MS spectra for DTE6-Et.

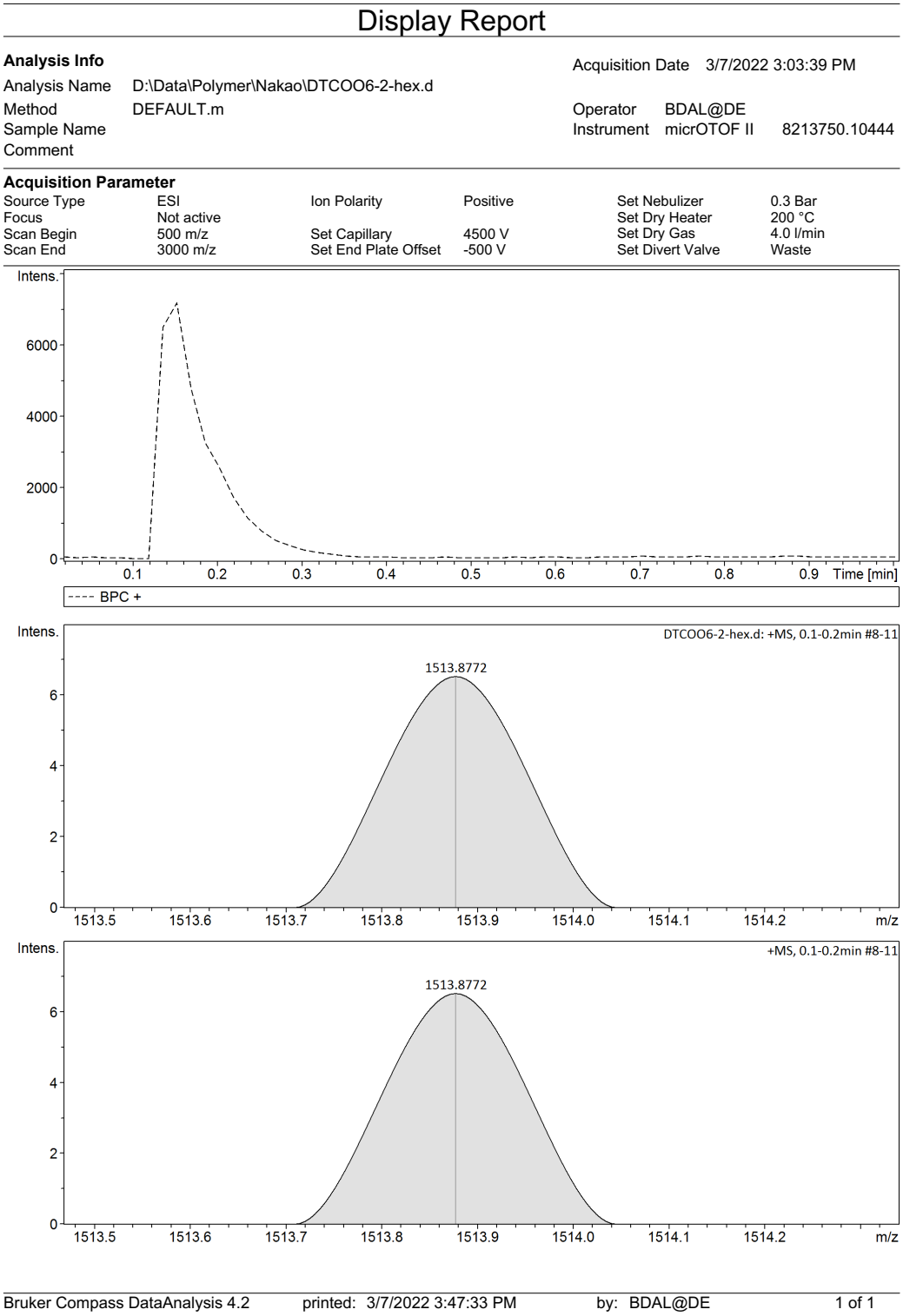

Figure S7 MS spectra for complexes DTE6-Hex.

4. Thermal properties

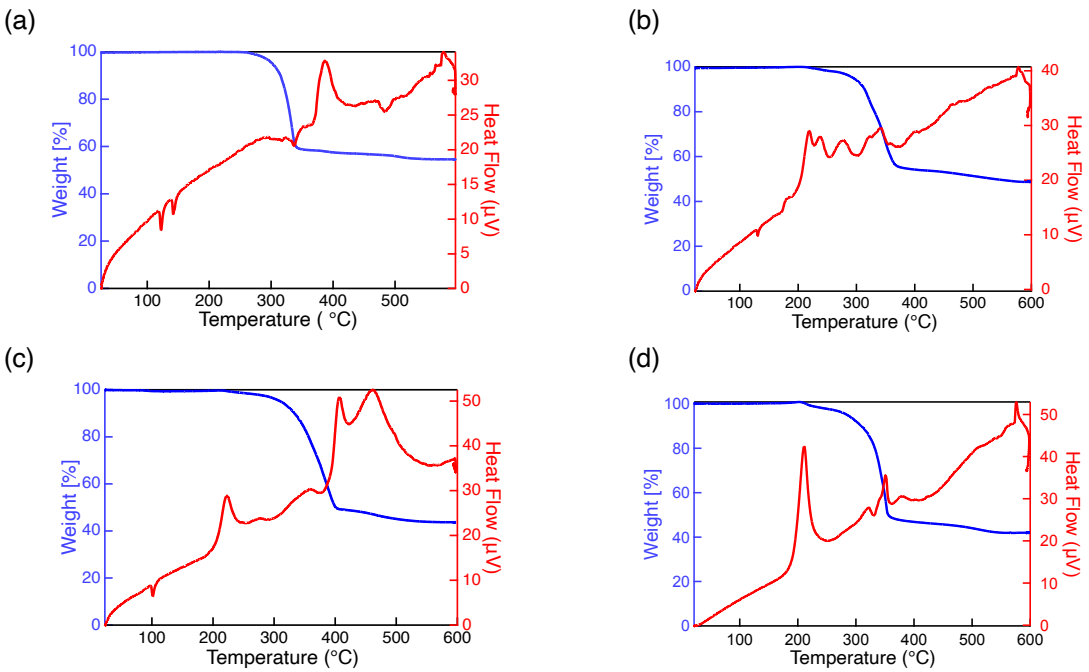

Figure S8. TG/DTA thermograms for the Au complexes: (a) **DT6**, (b) **DTE6-H**, (c) **DTE6-Et**, (d) **DTE6-Hex**. The measurements were performed at a scanning rate of 5 °C min^{-1}.

5. POM images

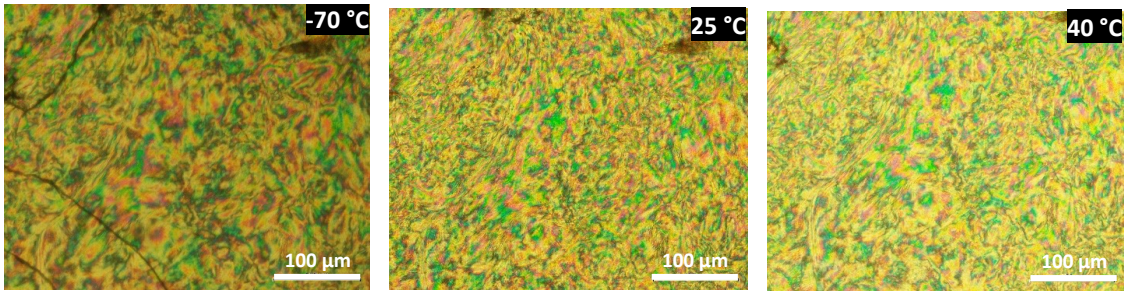

Figure S9. POM images of DTE6-Hex at variable temperature.

6. Powder X-ray diffraction (PXRD)

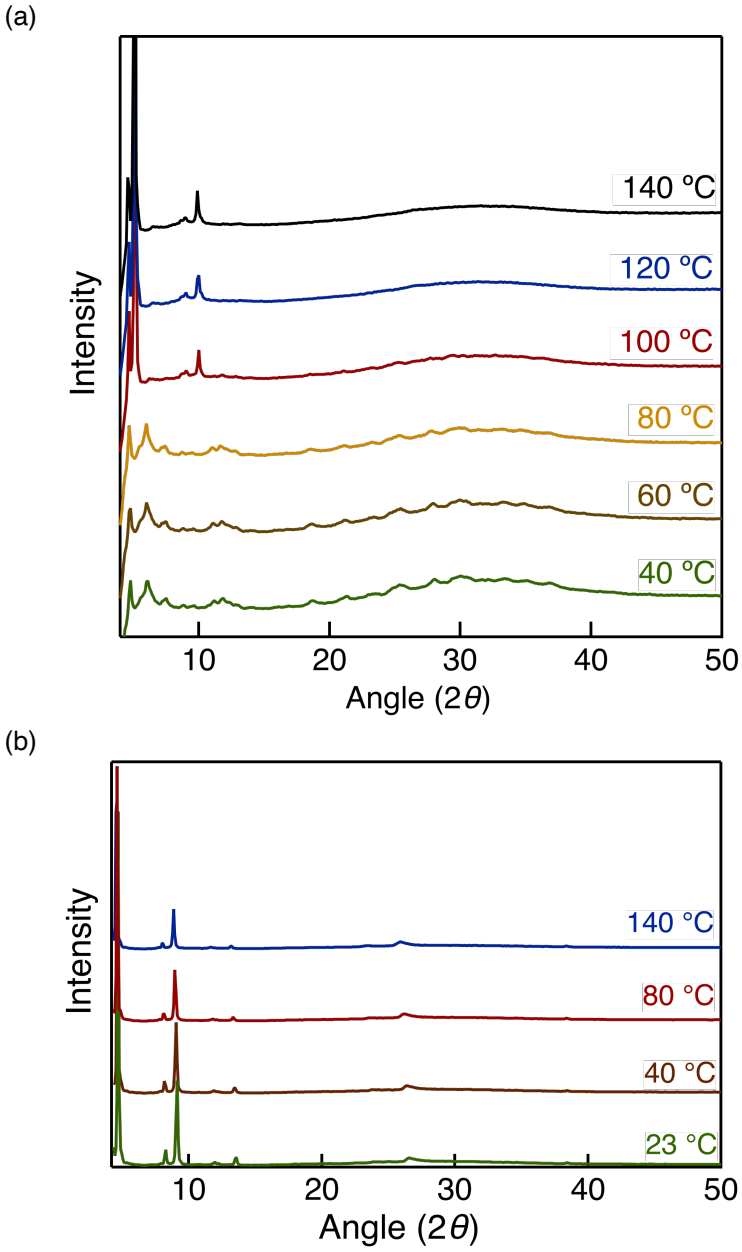

Figure S10. PXRD of complexes DTE6-R at variable temperatures: (a) **DTE6-Et** and (b) **DTE6-Hex**. Measurement temperatures are indicated in the figures.

7. Small angle X-ray scattering measurement (SAXS)

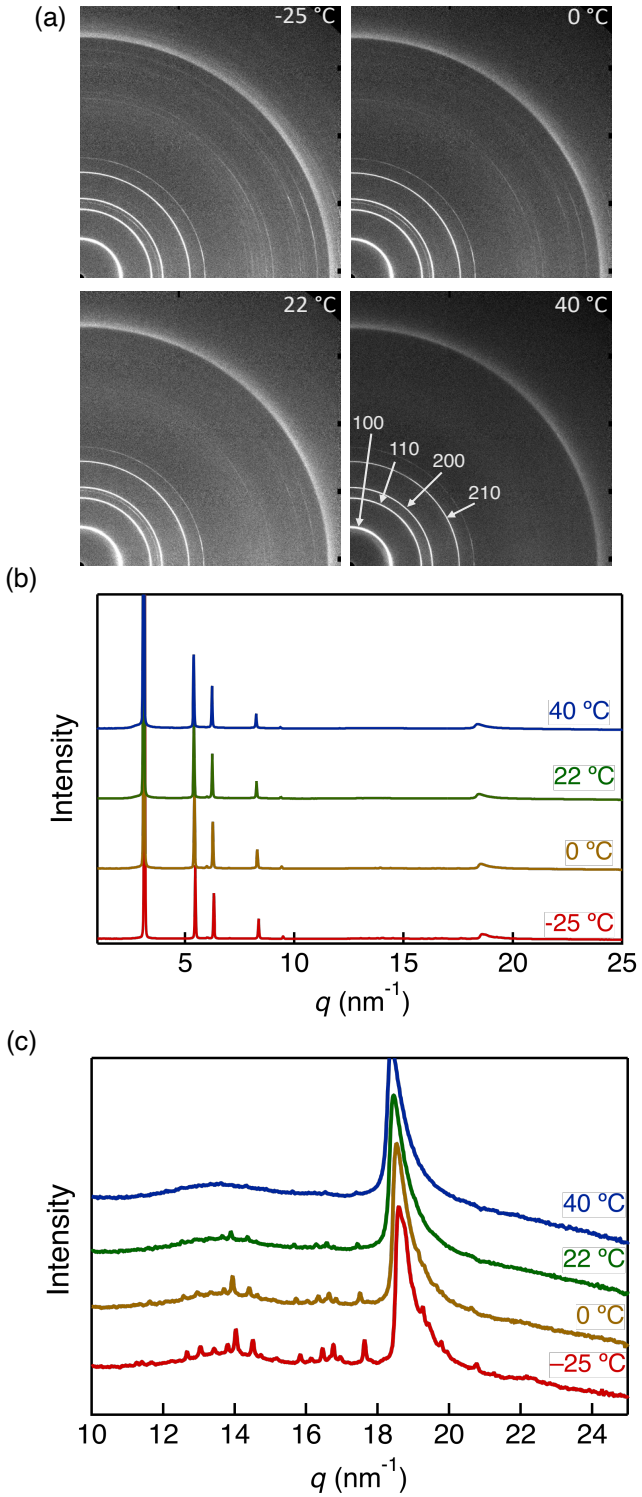

Figure S11. SAXS analysis of DTE6-Hex at variable temperatures. (a) Two-dimensional SAXS patterns recorded at –25, 0, 22, and 40 °C, with Miller indices assigned for the hexagonal columnar phase. (b) Radially averaged SAXS intensity profiles of full q-range. (c) Zoomed view of intensity profile with vertically offset for clarity. At 40 °C, four well-defined scattering peaks appear in the small-angle region with q-ratios of 1 : √3 : 2 : √7, consistent with a two-dimensional hexagonal columnar (Col_h) lattice indexed as (100), (110), (200), and (210).

Table S2. SAXS data and structural parameters for DTE6-Hex in the Col_h phase (40 °C)

q (nm $^{-1}$)	d (Å)	Index (hkl)	a_h (Å)[a]
3.1	20	(100)	23
5.5	12	(110)	23
6.3	10	(200)	23
8.3	7.6	(210)	23

[a] Calculated assuming a two-dimensional hexagonal lattice: $a_h = \left(2/\sqrt{3}\right) d_{hk0}\sqrt{h^2 + hk + k^2}$

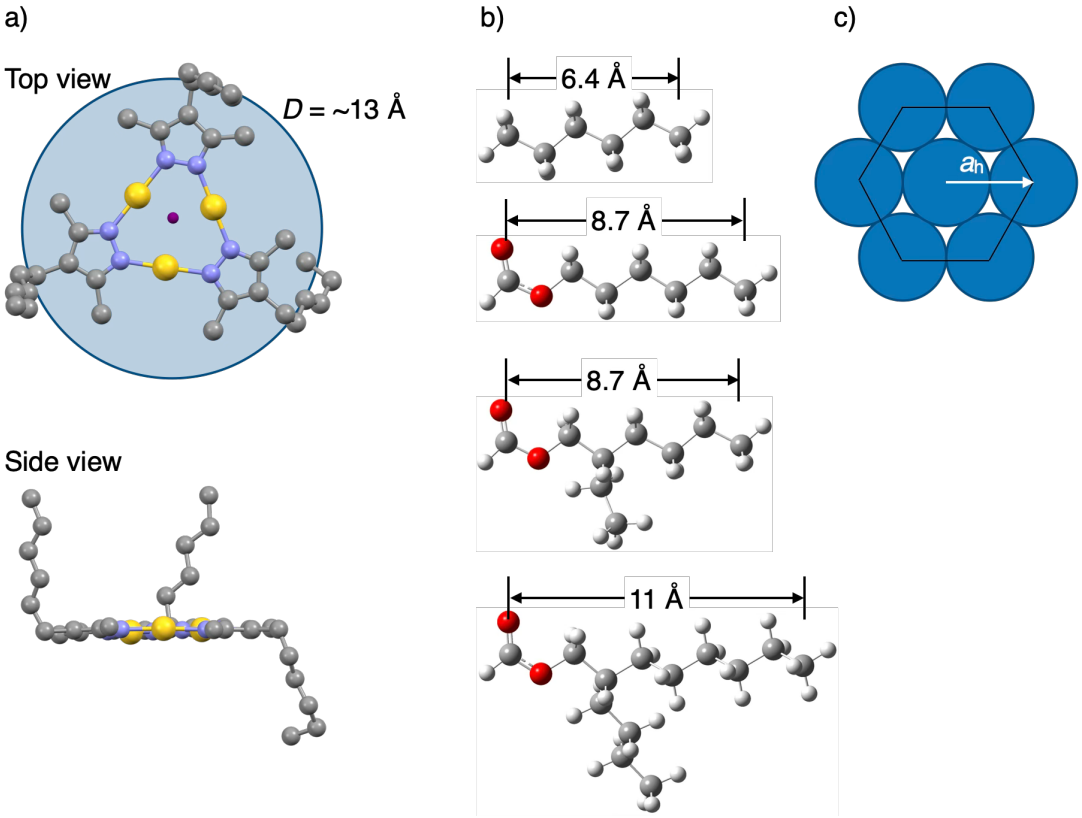

Figure S12. Structural considerations for hexagonal columnar packing in trinuclear Au complex systems. (a) Top and side views of the single-crystal X-ray structure of the previously reported DT6 complex, illustrating the effective disc-like molecular shape with an approximate diameter of ~13 Å. (b) Optimized molecular models of representative branched alkyl side chains connected via ester linkages, showing the estimated end-to-end distances of the alkyl segments. (c) Schematic illustration of hexagonal columnar packing, highlighting the hexagonal lattice parameter a_h. Colour code: Au, yellow; N, blue; C, grey; H, white; O, red; centroid of the trinuclear core, deep red.

8. Schematic illustration of phase sequence

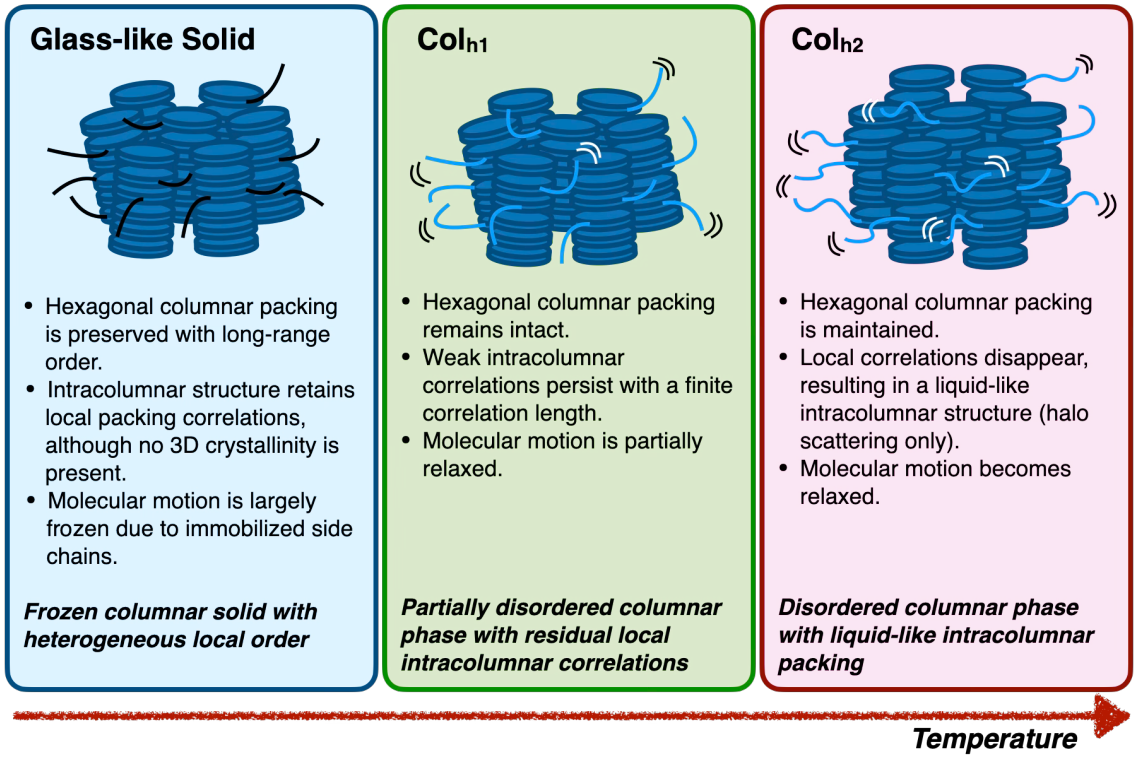

Figure S13. Schematic illustration of the hierarchical structural evolution of DTE6-Hex upon heating. The long-range hexagonal columnar order is preserved across all phases, while the intracolumnar local packing progressively diminishes from the glass-like solid state to Col_{h1} and finally to Col_{h2}. In the solid and Col_{h1} phases, short-range correlations give rise to correlation peaks in SAXS profiles, whereas in Col_{h2} only diffuse scattering remains, indicating the loss of local order. This highlights the decoupling between long-range positional order and local molecular packing.

9. Photoluminescence Properties

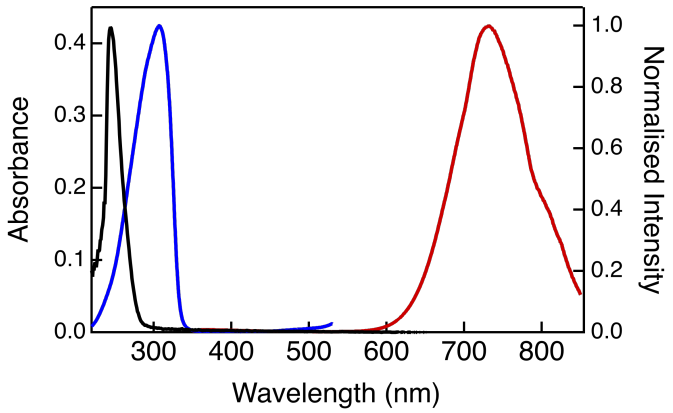

Figure S14. Photophysical properties of DTE6-Et: black, absorption spectrum in CH_2Cl_2 (5×10^{-5} mol L^{-1}); blue and red, excitation (blue, λ_{em} = 730 nm) and emission (red, λ_{ex} = 300 nm) spectra in crystal at 23 °C.

10. Photoluminescence lifetime

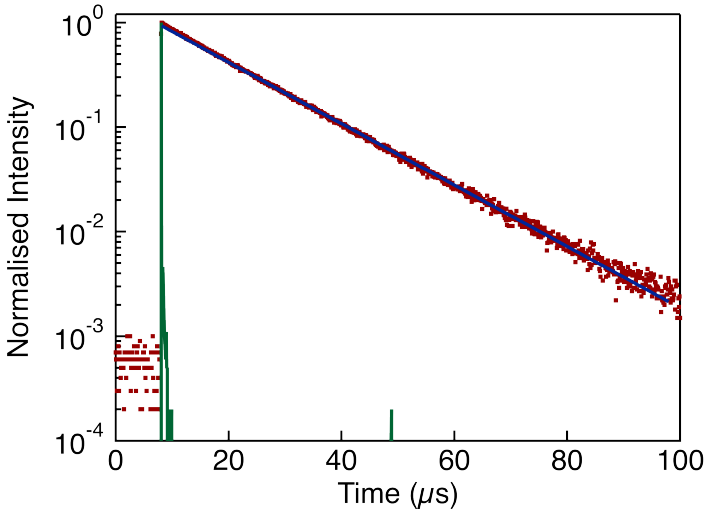

Figure S15. Luminescence decay profiles of DTE6-Et in condensed phases at 25 °C in air: (red, observed luminescence decay; blue, fitting curve; black, instrument response function). The decay was monitored at 730 nm for DTE6-Et by excitation at 280 nm.

11. Summary of Structure–property relationship

Table S3. Summary of structure–property relationship

complex	sidechain	LC phase	a_h (Å)	λ_{em}^{max} (nm)	Φ	τ (μs)
DTE6-H	hexyl	Col_{ho}	18.4	721	0.86	14
DTE6-Et	2-ethylhexyl	Col_h	19.9	731	0.49	15
DTE6-Hex	2-butyloctyl	Col_{h1}– Col_{h2}	21.7	741	0.36	14

12. Aggregation-Induced-Emission behaviour (AIE)

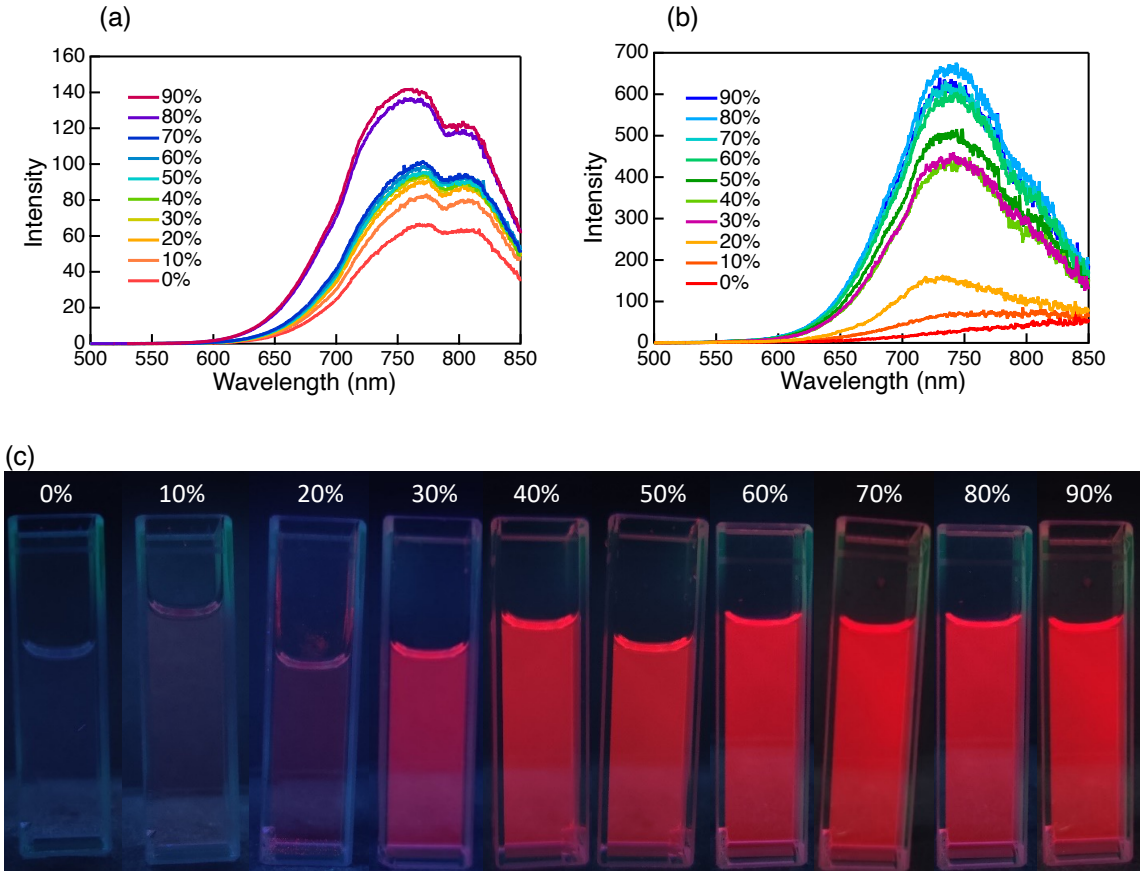

Figure S16. AIE behaviour of DTE6-R complexes in THF/water mixed solvent systems. (a) Photoluminescence spectra of DTE6-H and (b) DTE6-Et recorded in THF/water mixtures with varying water volume fraction (f_w = 0–90%) at a concentration of 5.0 × 10^{-5} mol L^{-1} (λ_{ex} = 300 nm). (c) Photographs of DTE6-Hex solutions at different water fractions taken under UV irradiation at 254 nm. Increasing water content induces aggregation of the complexes, leading to a pronounced enhancement of emission intensity, characteristic of aggregation-induced emission.

13. Temperature dependence luminescence

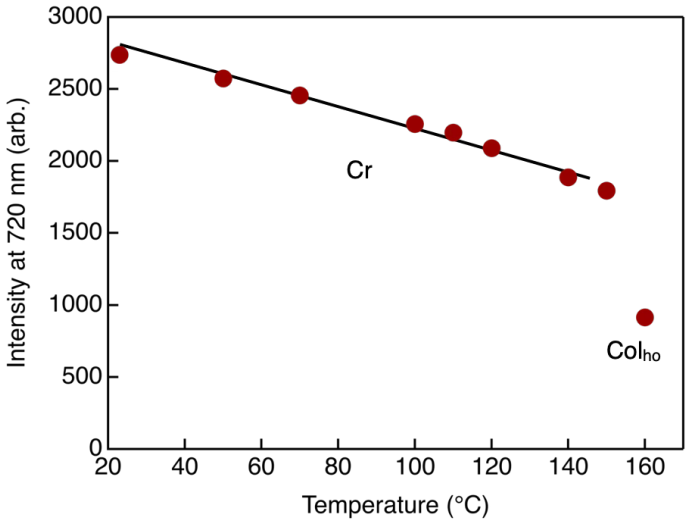

Figure S17. Temperature dependence of the photoluminescence intensity at 720 nm for DTE6-H during the heating process (λ_{ex} = 300 nm). In the crystalline (Cr) phase, the emission intensity decreases gradually with increasing temperature, reflecting thermally activated nonradiative deactivation. At the crystal-to- Col_{ho} phase transition, a pronounced and discontinuous drop in emission intensity is observed, indicating a substantial change in the aggregated emissive environment associated with the formation of the ordered hexagonal columnar mesophase.

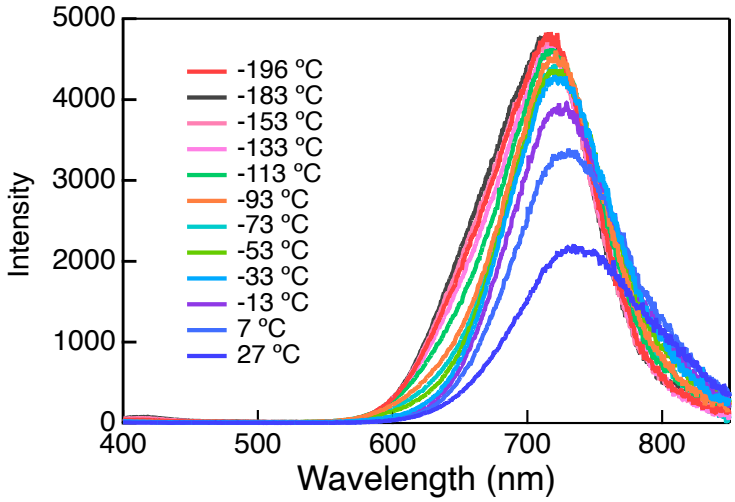

Figure S18. Low-temperature photoluminescence spectra of DTE6-Hex (λex = 300 nm) recorded during the heating process from -196 °C to 27 °C. Measurement temperatures are indicated in the figure. At -196 °C , DTE6-Hex exhibits enhanced emission intensity with a blue-shifted maximum, reflecting suppression of structural relaxation and nonradiative decay in the low-temperature solid state. Upon heating, the emission maximum gradually red-shifts and the spectral profile recovers to that observed at room temperature, consistent with thermally activated relaxation of the aggregated emissive structure.

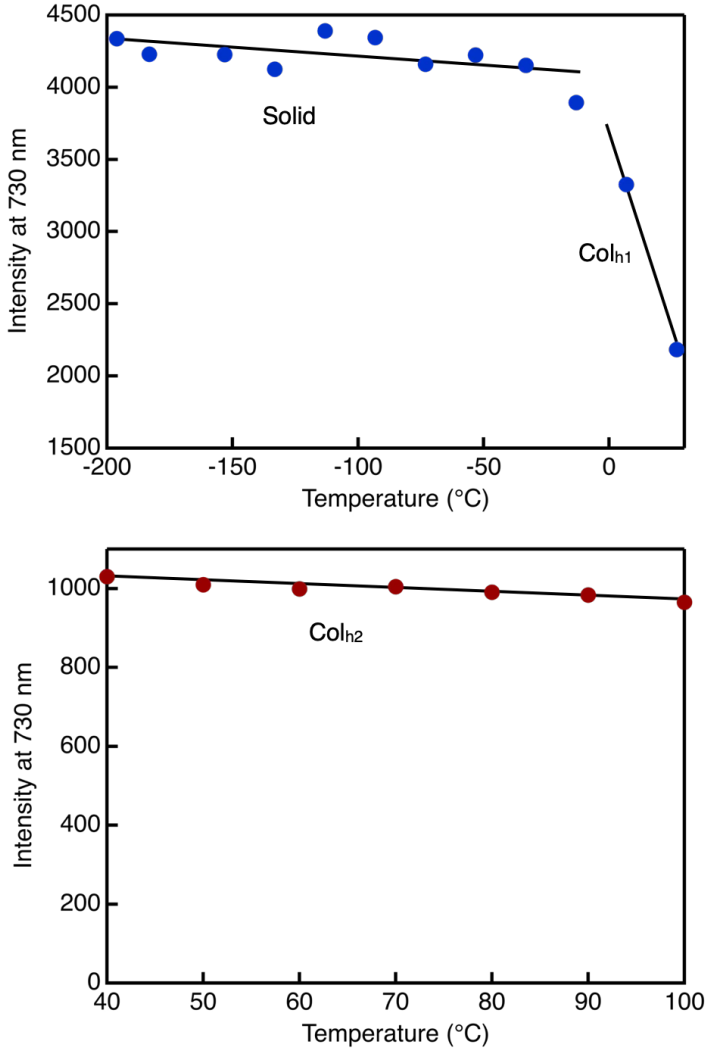

Figure S19. Temperature dependence of photoluminescence intensity of DTE6-Hex monitored at 730 nm (λ_{ex} = 300 nm). (Top) Cryogenic to near-room-temperature region, showing the solid and Col_{h1} phases. The emission intensity is nearly temperature-independent in the LC-like solid state down to –196 °C but decreases steeply upon heating across the solid-to-Col_{h1} transition at ca. –15 °C. (Bottom) High-temperature region corresponding to the Col_{h2} phase. The emission intensity remains nearly constant upon heating from 40 to 100 °C, indicating a thermally robust emissive state in the fully disordered hexagonal columnar mesophase.

14. POM images after shearing

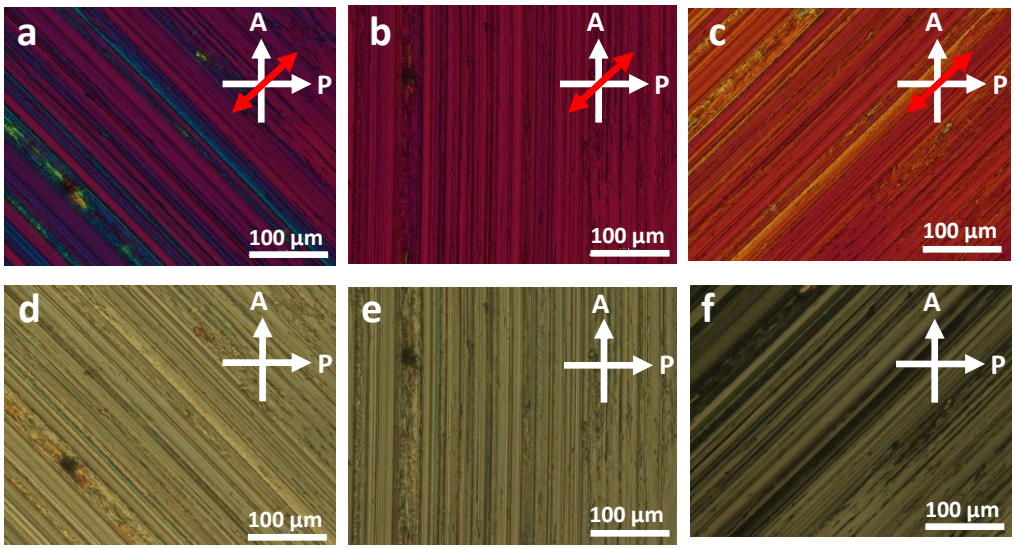

Figure S20. POM images of unidirectional aligned sample DTE6-Hex, (a) rotated by -45° (b) parallel to the analyser (c) rotated by +45° with colour sensitivity plate (R = 530 nm). (d) rotated by -45° (e) parallel to the analyser (f) rotated by +45° without colour sensitivity plate. White arrows indicate the direction of polarizer and analyser in POM. Red arrows indicate the optical axis of colour sensitivity plate.

15. DFT Calculation

Computational calculations were performed for the model complexes **DT1** and **DTE1** using density functional theory (DFT) with the B3LYP hybrid functional and the 6-311+G(d,p) basis set for H, C, N, and O atoms or the SDD basis set for Au atoms.

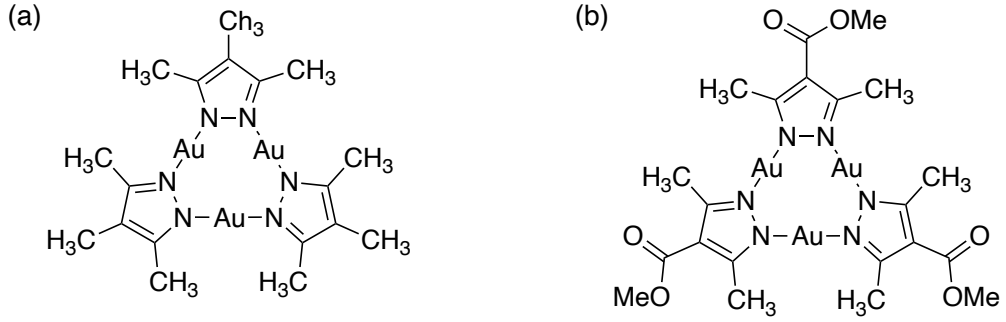

Figure S21. Molecular structures of model complexes used for the computation: (a) **DT1** as a model for **DT6**, (b) **DTE1** as a model for **DTE6-R**.

Table S4 Transition, oscillator strength (*f*), and excitation wavelength (*λ*) calculated for the monomer of the trinuclear Au complex.

Complex	Transition[1]			*f*	*λ* (nm)
DT1	HOMO	→	LUMO+3 (LMCT)	0.0629	244.12
	HOMO–1	→	LUMO+3 (LMCT)	0.0504	243.57
DTE1	HOMO–1	→	LUMO+1 (LMCT)	0.0789	239.11
	HOMO	→	LUMO+1 (LMCT)	0.0802	239.10
	HOMO–3	→	LUMO (MC)	0.3461	236.37
	HOMO–4	→	LUMO (MC)	0.3442	236.36

[1]LMCT: ligand-to-metal charge transfer transition, MC: metal-centred transition.

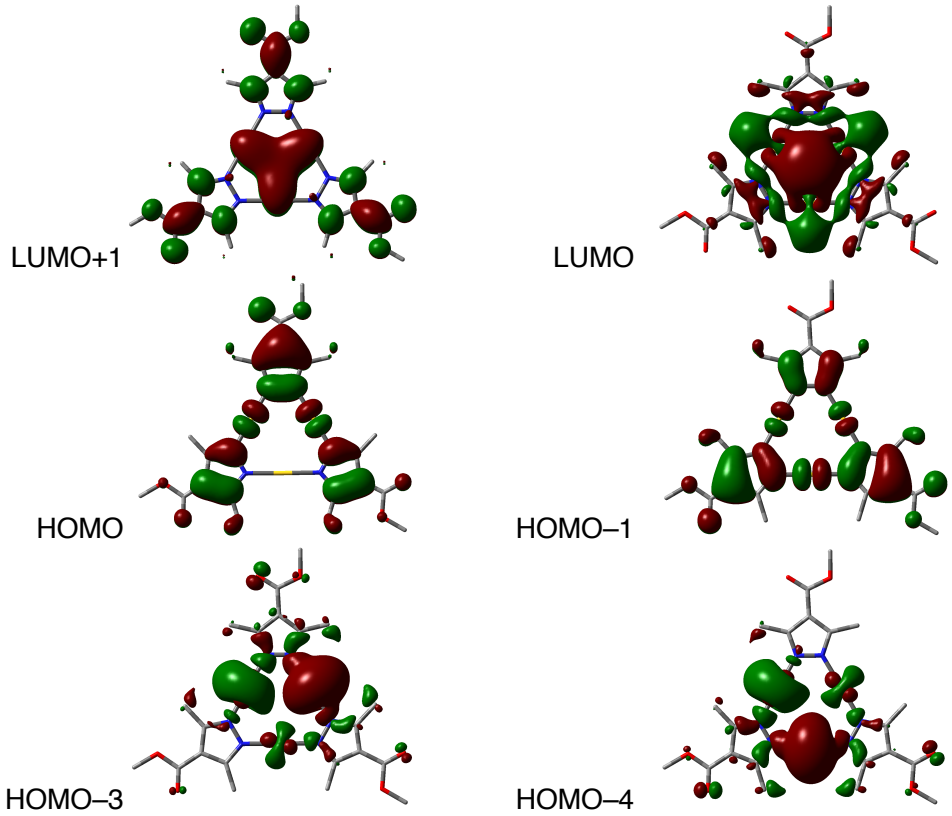

Figure S22. Molecular orbitals of the **DTE1** monomer obtained by DTF calculation. For clarity, the H atoms are omitted. Atom colour legend: grey, C; blue, N; red, O; yellow, Au.